Mn *K*-edge XANES studies of $La_{1-x}A_xMnO_3$ systems (A=Ca, Ba, Pb)

F. Bridges,[1] C. H. Booth,[2] M. Anderson,[1] G. H. Kwei,[2] J. J. Neumeier,[3] J. Snyder,[4] J. Mitchell,[5] J. S. Gardner,[2] and E. Brosha[2]

[1]*Physics Department, University of California, Santa Cruz, California 95064*
[2]*Los Alamos National Laboratory, Los Alamos, New Mexico 87545*
[3]*Physics Department, Florida Atlantic University, Boca Raton, Florida 33431*
[4]*JPL, California Institute of Technology, Pasadena, California 91109-8099*
[5]*Argonne National Laboratory, Argonne, Illinois 60439*

(Received 1 February 2000; revised manuscript received 23 August 2000; published 1 May 2001)

We present Mn *K*-edge x-ray absorption near-edge structure (XANES) data for a number of manganite systems as a function of temperature. The $1s$ absorption edge for the Ca-substituted samples is very sharp, almost featureless, and shifts uniformly upwards with increasing Ca content. The interpretation of this result is controversial because the lack of structure appears difficult to reconcile with a mixture of Mn^{+3} and Mn^{+4} ions or with several different Mn-O bond lengths at high T. We propose a possible solution in terms of covalency and considerable overlap of the Mn p states (mostly Mn $4p$). The manganite preedge structure is quite similar to that for a large number of other Mn compounds, with two or three small peaks that are ascribed to $1s$-$3d$ weakly allowed dipole transitions plus possibly a small quadrupole component. The weak dipole transitions are explained as arising from a hybridization of the Mn $4p$ state of the excited atom with an odd symmetry combination of Mn $3d$ states on adjacent Mn atoms. The first preedge peak A_1 has a small shift to higher energy with increasing valence while the next peak A_2 is nearly independent of dopant concentration at 300 K. However, for the colossal magnetoresistance (CMR) samples the A_2 preedge peak shifts to a lower energy below the ferromagnetic transition temperature T_c, resulting in a decrease in the A_2-A_1 splitting by $\sim$0.4 eV. This indicates a change in the higher-energy $3d$ bands, most likely the minority spin e_g, plus some change in covalency. In addition, the amplitudes are temperature dependent for the CMR materials, with the change in A_1, A_2 correlated with the change in sample magnetization. For the charge ordered (CO) sample, the analysis suggests that the change in the preedge is produced by a distortion that increases below T_{CO}. We discuss these results in terms of some of the theoretical models that have been proposed and other recent XANES studies.

DOI: 10.1103/PhysRevB.63.214405 PACS number(s): 75.70.Pa, 61.10.Ht, 71.38.−k, 72.20.Jv

I. INTRODUCTION

The $La_{1-x}A_xMnO_{3+\delta}$ systems exhibit a wide range of phenomena depending on the divalent atom (A) concentration, x, (A=Ca, Ba, Sr, Pb, etc.), and the O concentration. These include ferromagnetism, antiferromagnetism, charge ordering, a metal-insulator transition, and large magnetoresistance effects.[1–6] For x in the range $\sim$0.2–0.5, these systems have a ferromagnetic transition at a temperature T_c, a metal/insulator transition (MI) at $T=T_{MI}$, and a ''colossal'' magnetoresistance (CMR) that reaches its maximum at T_{MR}, with $T_{MI}\sim T_{MR}\sim T_c$ in many cases. The substitution of a divalent ion for La^{+3} formally changes the average Mn valence to $3+x$ (the Mn valence is $+3$ in $LaMnO_3$ and $+4$ in $CaMnO_3$) and is usually thought to introduce holes into the narrow e_g band of Mn $3d$ electrons that are also hybridized with O $2p$ states. It is the changing occupation of this hybridized band with x that leads to many of the observed properties. Excess O in $LaMnO_{3+\delta}$ (actually Mn and La vacancies) or La vacancies can also increase the formal Mn valence, thereby adding carriers to the system.

The coupling between charge and magnetism has been modeled using the double exchange mechanism[7–9] plus strong electron-phonon coupling.[10–12] In the ferromagnetic metallic state, well below T_c, the charge carriers are assumed to be highly delocalized (large polarons) and spread out over several unit cells for CMR samples.

In the paramagnetic state above T_c for CMR samples, there is a significant increase in the distortions about the Mn atoms compared to the low-temperature data.[13–17] This distortion is generally attributed to the charge carriers becoming partially localized on the Mn atoms. However, mobile holes could also be located more on the O atoms as is the case for cuprates.[18] Consequently, there might be very little change in the charge localized on the Mn atoms above and below T_c. This raises the question as to how the energy shift of the absorption edge relates to valence and the local environment in these materials. Is there a mixture of ''ioniclike'' $+3$ and $+4$ states, an average valence, as in a metal where all Mn atoms are equivalent, or something in between? Do band-structure effects play a role?

Experimentally,[15,16,19] the Mn *K*-edge for the Ca-substituted manganites is sharp, with relatively little structure, and shifts almost uniformly with dopant concentration, consistent with an average valence state of $v=3+x$. The sharpness of the edge is suggestive of a transition into a Mn state that is uniform throughout the sample, and previously we and others have interpreted this result to mean that all Mn sites have comparable local charge densities.[15,16,19] This sharpness is difficult to reconcile with the usual assumption of a mixture of purely *local* ionic Mn^{+3} and Mn^{+4} sites. For example, we show explicitly (Sec. IV A) that the observed *K* edge cannot be modeled as a weighted sum of the edges of

the end compounds $LaMnO_3$ and $CaMnO_3$ for the CO material with 65% Ca. A similar result has already been noted for CMR materials.[16] In addition, Tyson *et al.*[20] have investigated the K_β emission that probes Mn $3d$ states through the $3p$-$1s$ decay, and they report that these spectra for the substituted manganite materials can be modeled as a weighted sum of the end compounds although the shifts with valence are rather small.

Pickett and Singh using the local spin-density approximation[21] (LSDA model) suggest that these systems are half metallic, with a gap between the O band and a minority-spin *d* band. They also point out that near 25% Ca, all Mn sites could be essentially identical (which would agree with the various *K*-edge studies) if the Ca were uniformly distributed such that there are two Ca and six La second neighbors to each Mn. Thus for the concentration range 20–30%, the local environment for each Mn may be very similar. Anisimov *et al.*[22] and Mizokawa *et al.*[23] suggest that a large fraction of the *d* electrons are found on the Mn atoms rather than transferred to the O atom as in an ionic solid (thereby leaving holes in the O band). These calculations yield similar electron densities on each Mn atom for sites associated with formal Mn^{+3} and Mn^{+4} valences. Other recent papers[24–27] have also stressed the importance of O, and the question of charge localization on the O atoms[28] or on the Mn atoms has been considered.

However, there remains a problem in understanding the edge, because there are significant changes in the local structure of the CMR materials. When the bond length of a molecule lengthens, the position of the edge shifts to lower energy;[29] this effect has been observed in many polarized x-ray-absorption fine-structure (XAFS) experiments. For the magnitude of the distortions present in the manganites, both Elfimov *et al.*[30] and Benfatto *et al.*[31] calculate using different methods that the edge should shift about 2 eV between the long and short bonds. Thus from this perspective there should be structure in the edge indicative of two edges (for long and short bonds) and this structure should change with *T*. However, we find no net shift of the edge through the transition to within 0.04 eV for any of the samples.

We will show using a careful subtraction technique, that there is in fact a tiny structural change that correlates with T_c for CMR samples, and hence with changes in the local structure, but the reason why it is nearly averaged out is not clear. We propose, based on recent calculations,[30] that this is a result of the strong overlap of Mn *p* states (dominated by the Mn $4p$ band within a tight-binding model) at the absorption edge, which averages over several Mn atoms as a result of band-structure effects. Since such effects are usually ignored in studies of the absorption edge, we describe this approach in more detail in the Sec. IV. A similar subtraction analysis of the CO sample data shows that the structure in the difference data is inverted relative to the CMR samples, and hence suggests an increased distortion for this sample below T_{CO}.

The preedge structure for the Mn *K*-edge consists of two or three small peaks labeled A_1–A_3, which have Mn $3d$ character. These features are observed for all the transition metals and are generally ascribed to mixtures of $1s$-$3d$ quadrupole and $1s$-$3d$ dipole transitions (weakly allowed by a hybridization between $3d$ states and $4p$ states). Although the latter are assumed to be dominant, the interpretation of the A_1 peaks is still controversial.[32] Two important issues are (1) how large is the quadrupole contribution and when it is important and (2) how are the dipole transitions made allowed when in many instances the local environment has inversion symmetry, and in that case[33] the transition is symmetry forbidden. There have been a large number of papers in the last five years addressing these issues for many of the transition metals, not all of which are in agreement. However some questions have been answered. Since quadrupole-allowed preedge features have a strong angular dependence, in contrast to the dipole-allowed transitions, measurements on single crystals as a function of angle can separate the two contributions. Such studies have shown that quadrupole transitions contribute to the A_1 peaks in Ti,[32,34] V,[35,36] Ni,[37] and Fe,[37] with the largest contribution at the lowest energies of the preedge. The amplitude can be as large as $\sim$4% of the absorption edge height for some systems at optimum orientations; but more generally it is of the order 1%, and would be smaller in powdered samples that are orientational averages. The dipole-allowed A_1 peaks are often in the 5–15 % range and often do dominate, but not always. For example, for Ti in rutile (TiO_2), the small A_1 peak appears to be primarily a quadrupole feature.[32]

Early Mn XANES work[33,38] assumed that the A_1–A_2 splitting is produced by the crystal-field parameter, often called the $10Dq$ parameter, which splits the t_{2g} and e_g states. These investigations did not consider the possibility of a large on-site Coulomb term *U*. Recent work, using the LSDA or the local-density approximation (LDA) with and without U, and including the Hund's rule exchange parameter J_H, find a Coulomb splitting of both the t_{2g} and e_g states, with the e_g states further split by the Jahn-Teller (J-T) interaction.[39]

Some promising calculations for considering the preedge features are those of Elfimov *et al.*[30] These calculations indicate that in addition to U and J_H, there are appreciable higher-order Coulomb terms that must be included and that strong hybridization occurs between the Mn $4p$ orbitals and the Mn $3d$ states on neighboring Mn atoms. The resulting splitting of the majority and minority e_g spin states results in a splitting of the Mn preedge features. We consider these calculations together with some of the new results on preedges in the discussion section.

In this paper we also investigate the preedge structure using a subtraction technique and find a temperature dependence that correlates with T_c for all CMR samples and with T_{CO} for the CO sample. The structure in the difference data for the CO sample is again inverted relative to the CMR samples. The splitting of the preedge peaks decreases in the ferromagnetic phase for the CMR samples, which may indicate a change in covalency.

In Sec. II we summarize the samples and experimental setup; some details were given earlier.[15] Then in Sec. III, we provide a more extensive discussion of the shift of the Mn *K*-edge as a function of concentration and temperature. Here we also present the preedge results. We consider the implications of these results in Sec. IV.

II. EXPERIMENTAL DETAILS

Many samples are used in this study, with the average Mn valence changed in a variety of ways: divalent substitutions for La^{+3} and changes in the La^{+3} or O concentrations. Powder samples of $La_{1-x}A_xMnO_3$ were prepared by solid-state reaction of La_2O_3, MnO_2, and a dopant compound $CaCO_3$, PbO, BaO for various divalent atoms *A*. Ca substitutions are $x=0.0$, 0.12, 0.21, 0.25, 0.3, 0.65, and 1.0, and Ba and Pb are 0.33. Several firings with repeated grindings were carried out using temperatures up to 1400 °C, with in some cases a final slow cool at 1 °C per minute. The dc magnetization was measured using a commercial superconducting quantum interference device (SQUID) magnetometer. The end compounds $CaMnO_3$ and $LaMnO_{3.006}$ show antiferromagnetic transitions at ~130 and 125 K, respectively, while the $x=0.65$ sample showed features consistent with a CO transition at 270 K and an antiferromagnetic transition at ~140 K.[5,6] Similar measurements on the substituted manganites indicate that they are all orthorhombic. The average Mn valence for several Ca-substituted samples was also determined by titration (Sec. III A). See Refs. 14,15 and 40 for further details.

The $LaMnO_{3.006}$ sample was prepared by grinding stoichiometric amounts of La_2O_3 and MnO_2 under acetone until well mixed. The powder sample was formed into a $\frac{3}{4}$ in. diameter pellet using uniaxial presure (1000 lb) and fired in an Al_2O_3 boat under pure oxygen for 12 h at 1200–1250 °C. Next the sample was cooled to 800 °C, reground, repelletized, and refired at 1200–1250 °C for an additional 24 h. This process was repeated until a single phase, rhombohedral x-ray diffraction trace was obtained. The reground powder was placed in an Al_2O_3 boat and post annealed in ultra-high purity Ar at 1000 °C for 24 h. The oxygen partial pressure was about 60 ppm (determined using an Ametek oxygen analyzer). The sample was then quenched to room temperature. Diffraction, titration, and thermogravimetric analysis (TGA) measurements indicated that this sample was essentially stoichiometric, with an oxygen content of 3.006.

Additional $LaMnO_{3+y}$ specimens with various average Mn valences were prepared at 1300 °C in air, followed by three intermediate regrindings. The original specimen was removed from the furnace at 1300 °C and had a Mn valence of 3.150. A piece of this specimen was reacted overnight at 1000 °C and removed from the furnace, producing a sample with an average Mn valence of 3.206. A nearly stoichiometric specimen with an average Mn valence of 3.063 was prepared at temperatures up to 1350 °C with four intermediate regrindings in flowing helium gas. Finally, the nonstoichiometric $La_{0.9}MnO_3$ specimen was prepared at temperatures of up to 1350 °C with three intermediate regrindings. It was slow cooled in air at 1.5 °C/min to room temperature and had an average Mn valence of 3.312. For each of these samples the valence was determined by titration.

A sample that should have isolated Mn^{+3} and Mn^{+4} species is also needed for comparison purposes; such a material is $Sr_3Mn_2O_{6.55}$.[41] The two species are due to the oxygen defect structure that puts vacancies into the MnO_2 planes to form mixtures of square pyramids and octahedra. This highly insulating material can then be understood from chemical reasoning to be Mn^{+3} (square pyramids) and Mn^{+4} (octahedra). Some further justification for this assignment comes from the compound $Ca_2MnO_{3.5}$, which is all Mn^{+3} and has only square pyramids with vacancies in the MnO_2 planes; it is an ordered superstructure of the single-layer compound.[42] $Sr_3Mn_2O_{6.55}$ was synthesized by firing a stoichiometric mixture of $SrCO_3$ and MnO_2 at 1650 °C for 12 h followed by rapid quenching into dry ice. This procedure is essential to prevent decomposition into α-Sr_2MnO_4 and $Sr_4Mn_3O_{10}$ on cooling and to prevent oxidation to $Sr_3Mn_2O_7$. The oxygen content was measured independently by iodometric titration and by thermogravimetric analysis, both techniques yielding 6.55(1) oxygen atoms per formula unit.

All XAFS data were collected at the Stanford Synchrotron Radiation Laboratory. Most Mn *K*-edge data were collected on beam line 2-3 using Si(220) double monochromator crystals for all samples. Some data were collected on beam line 4-3 using Si(111) crystals, while most of the Mn *K*-edge data for the Ba-substituted sample were collected on beam line 10-2 using Si(111) and (220). The manganite powders were reground, passed through a 400-mesh sieve, and brushed onto scotch tape. Layers of tape were stacked to obtain absorption lengths $\mu_{Mn}t\sim1$ (μ_{Mn} is the Mn contribution to the absorption coefficient and t the sample thickness) for each sample. Samples were placed in an Oxford LHe flow cryostat, and temperatures were regulated to within 0.1 K. All data were collected in transmission mode. A powdered Mn metal sample was used as an energy reference for each scan. The preedge absorption (absorption from other excitations) was removed by fitting the data to a Victoreen formula, and a simple cubic spline (7 knots at constant intervals ~140 eV in E) was used to simulate the embedded-atom absorption μ_0 above the edge.

The edge shifts are reported relative to a Mn powdered metal foil for which we took the position of the first inflection point to be 6537.4 eV.[16] For each scan, the position of the reference edge was determined by fitting the edge to that of a fiducial scan. This provided a correction to the relative edge position consistent within ±0.015 eV (see the next section).

In the preedge region there is a remnant of the La L_I XAFS that must be considered; the oscillation amplitude is about 0.3% of the Mn step height just before the preedge. However, the La *K*-edge XAFS showed that there is a ''beat'' in the XAFS from about 8.4–10 $Å^{-1}$, which for the La L_I XAFS corresponds to the range of the Mn XANES. In this beat region the La L_I XAFS is reduced by another factor of 4; thus the La oscillations underlying the Mn XANES region has an amplitude of about 0.08%, much smaller than the changes we investigated. In addition, this oscillation slowly varies with energy, and would have at most produced a slowly varying background. Consequently any remaining La L_I XAFS is not a problem for the Mn XANES study.

III. NEAR-EDGE RESULTS

A. Main edge

In Fig. 1 we show the Mn absorption *K* edge for several concentrations of Ca, 33% Ba and Pb,

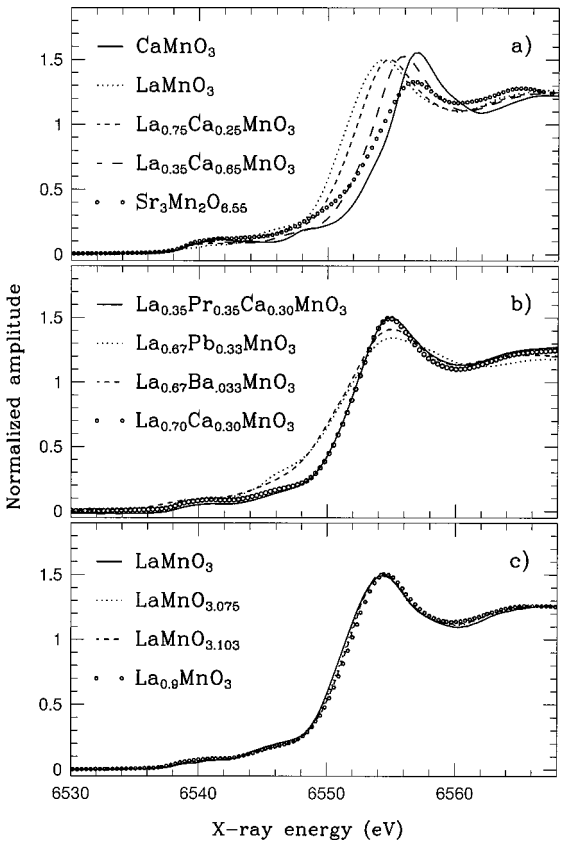

FIG. 1. The Mn *K*-edges for a number of similar manganite systems, corrected for energy shifts of the monochromator (see text).

$La_{0.35}Pr_{0.35}Ca_{0.3}MnO_3$, a $Sr_3Mn_2O_{6.55}$ sample that should have a nearly uniform mixture of ionic Mn^{+3} and Mn^{+4}, some O-excess samples, and a La-deficient sample.

For the Ca substituted samples this figure shows that (1) to first order the main absorption edges (ignoring preedge structures for now) have almost the same shape for each dopant concentration and shift nearly rigidly to higher energy as the concentration is increased, (2) the edges for the manganite samples are very sharp, roughly half as wide as the edge for the $Sr_3Mn_2O_{6.55}$ sample, (3) there is no obvious kink or structure in the sharp edges for the substituted (La,Ca) manganite samples that would indicate a simple mixture of Mn^{+3} and Mn^{+4} ions, and (4) there is a tiny shape change, however, visible in Fig. 1 for samples of different concentrations, that shifts the *position* of the inflection point on the edge relative to the half height position.

The data for the $La_{0.35}Pr_{0.35}Ca_{0.3}MnO_3$ sample looks very similar to that for $La_{0.7}Ca_{0.3}MnO_3$ indicating that replacing some of the La by Pr does not change the local electronic configuration on the Mn. The O-excess and La-deficient samples show a similar edge shape to $LaMnO_3$, but the edge shift is considerably smaller than expected based on the Mn valence obtained from TGA. The shifts for the O-excess data are inconsistent with data from other groups[43,44] and are included here to show the sharpness of the edge. However, such data suggest that the position of the Mn *K*-edge is determined by several factors and using the Mn valence and O-content obtained from TGA may not be sufficient.

In contrast to the Ca-substituted materials, Ba and Pb substitution results in a significantly broader edge, more comparable to the edges of other Mn oxides[33,45,46] and the $Sr_3Mn_2O_{6.55}$ sample. There is relatively more weight in the lower part of the edge.

In addition to the shift of the inflection point position on the edge with Ca concentration, as noted above, the region of steepest slope is also quite broad. Consequently using the position of the peak in the first derivative curve as a measure of the average edge position (as we and others have done previously) is only an approximate measure of the average edge shift. Using the derivative peak yields a roughly linear shift with concentration.[15,16,19] Our data and that of Subías *et al.*[16] have the same edge shift per valence unit, while the shift reported by Croft *et al.*[19] is smaller. This may be the result of different O content in the samples.

To obtain a better estimate of the average edge shift with concentration (at room temperature), we have fit the $LaMnO_3$ edge data (or the $CaMnO_3$ data) to that for each of the other samples over the main part of the edge (above the preedge structure). In this procedure it is important that when the absorption from other atoms is removed, the data baseline below the preedge structure be at zero. Each edge is also normalized using some feature of the data; for the data at different concentrations, we normalized over a range of energies well above the edge, where the XAFS oscillations are small. Similarly we fit the corresponding reference edges (Mn foil) to a reference scan to obtain a net overall edge shift. Several examples of these fits are shown in Fig. 2. Although there is a change in shape between $LaMnO_3$ and $CaMnO_3$, the relative shifts determined with either end compound are nearly identical—less than 0.02 eV difference over the entire concentration range.

In Fig. 3(a) we plot the relative shifts obtained from fits to $LaMnO_3$ at room temperature. The shift with x is roughly linear with concentration, with a net shift from 0–100 % Ca of ~ 3 eV. This is considerably smaller than the value 4.2 obtained from the derivative peak[15,16] and illustrates the effect of the shift of the inflection point relative to the half height. However, over the straight part of the plot from $x = 0.3$–1.0, the slope is 3.3 eV/valence unit, quite close to the 3.5 eV/valence unit obtained by Ressler *et al.*[47] for MnO, Mn_2O_3, and MnO_2. The point at $x = 0.12$ is anomalous, but titration measurements give about the same Mn valence for the 12 and 21% samples, which agrees with the comparable edge shifts observed. Figure 3b shows that the variation with valence is smoother, but slightly nonlinear. The different values for the titrated valence, compared to the value expected from the Ca concentration, likely indicates an O content variation.

We have also used a similar analysis to investigate any possible edge shift as a function of temperature by fitting the entire edge of the 50 K data for a given sample to all the higher-temperature data files. Two examples are shown in Figs. 2(c) and 2(d). The figures show that changes in the shape of the main edge above and below T_c are quite small (although measurable). The largest relative change is in the

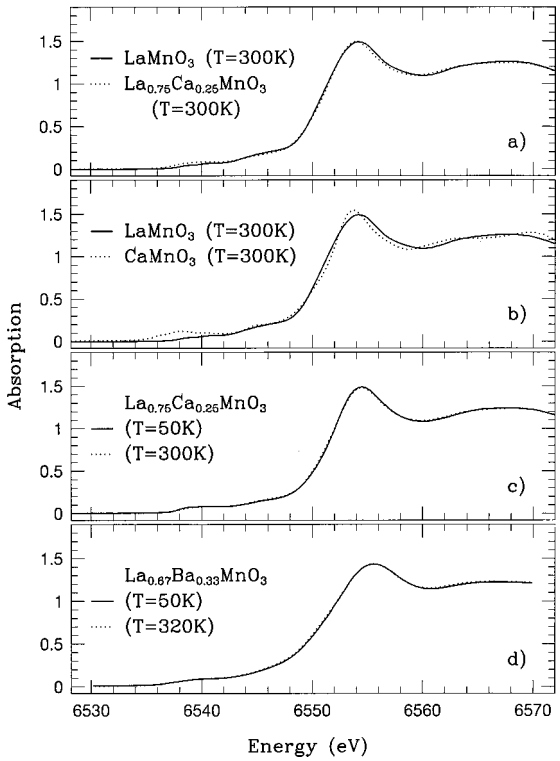

FIG. 2. Fits of absorption edges to each other. In (a) and (b) we show fits of the $LaMnO_3$ edge (solid curve) to the 25 and 100% Ca samples. In (c) and (d) we show fits of the 50 K data (solid curve) to high-temperature data for two different samples. Corrections from the Mn-foil reference not included.

preedge peaks, to be discussed later. In Fig. 4 we show the shift of the edge position as a function of temperature up to 320 K for several sets of samples. (We have similar data out to nearly 500 K for the Ba sample and $CaMnO_3$.) Variations in the fit values of the net shift ΔE_o for several traces at the same temperature are less than ± 0.02 eV, and fluctuations about the small average shift with T are comparable for a given experimental run. Differences between experimental setups or using Si<111> or Si<220> monochromators are less than 0.1 eV. For T less than 300 K, the net shift for each sample is very small (less than 0.04 eV), but nearly all appear to have a slight decrease at high T.

B. Preedge region

In Fig. 5 we plot the preedge region as a function of temperature on an expanded scale for $CaMnO_3$, a CMR sample with 21% Ca, and the 33%-Ba sample. Data for $LaMnO_3$, a CO sample with 65% Ca, and another CMR sample have recently been published[48] in a short paper. For these systems the main features are the lower three peaks labeled A_1–A_3 (near 6539, 6541, and 6544 eV) and the B peak. The lower two peaks A_1 and A_2 are common to all materials although not resolved for the 33%-Ba data collected using Si(111) crystals that have a lower-energy resolution. The comparison of the two Ba data sets in this figure illustrate the importance of using high-energy resolution. The A_3 peak is not obviously present in most samples. In

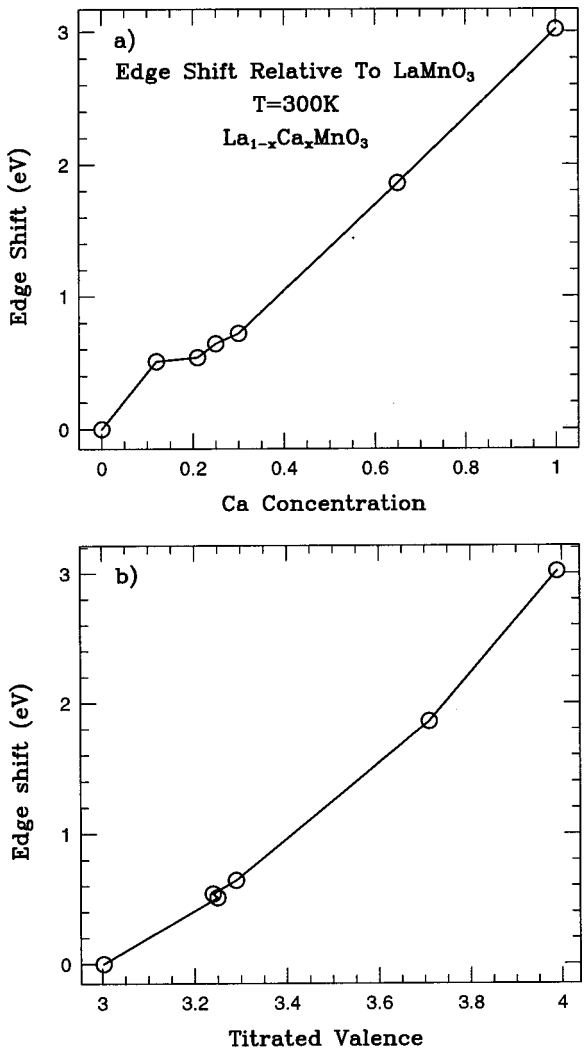

FIG. 3. The shift of the Mn K edge with (a) Ca concentration and (b) titrated valence for $La_{1-x}Ca_xMnO_3$. Note we do not have titration data for $x=0.30$. The relative errors are edge shift, ± 0.02 eV, and smaller than symbols; Mn valence ± 0.02 units and slightly larger than symbols. In this and several following figures, the lines are a guide for the eye only.

Fig. 6 we compare the data for the 30%-Ca CMR sample with the $Sr_3Mn_2O_{6.55}$ sample and also show the preedge for the Pb sample, all on a more expanded scale.

Note that all the preedge features start at very nearly the same position regardless of doping, and the amplitude of the preedge features labeled A increases with average Mn valence (Ca concentration) as observed in other Mn compounds[33] and in a previous manganite study.[19] There are, however, small shifts of these features with Ca concentration as shown in Fig. 7. The A_1 peak energy increases slightly from $LaMnO_3$ to $CaMnO_3$, and the A_1-A_2 splitting decreases from 2.2–1.8 eV. (The exception is the 65% sample, but here the A_i peaks are poorly resolved.) For the substituted samples, the leading edge of the A_1 peak remains steep for all concentrations except the 65% sample. Consequently, the preedge for the intermediate concentrations (CMR samples) cannot be modeled as a simple weighted sum of the end compounds $LaMnO_3$ and $CaMnO_3$. Note that the leading

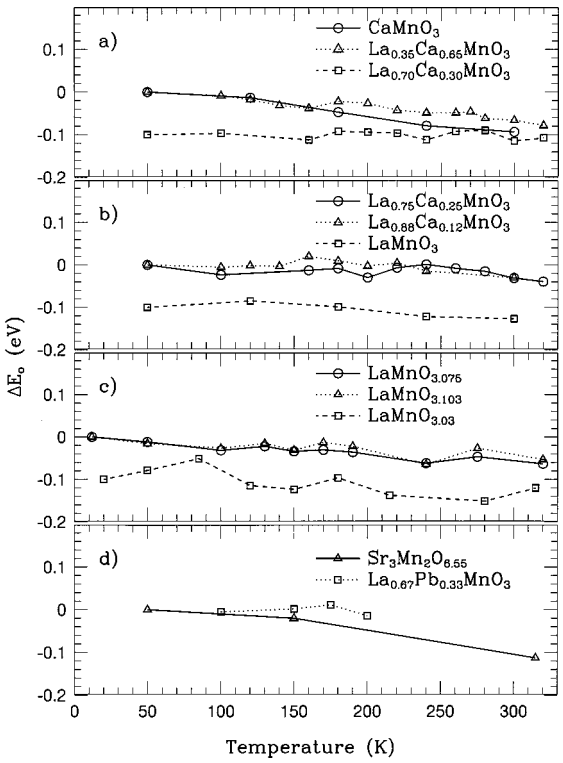

FIG. 4. The shift of the absorption edge for each sample relative to the low-temperature data. In panels (a)–(c), one of the curves (squares) is shifted downward by 0.1 eV for clarity. Relative errors are ± 0.015 eV and ± 0.03 eV for $LaMnO_{3.03}$.

edge for the $Sr_3Mn_2O_{6.55}$ sample (see Fig. 6) is broader, consistent with a mixture of Mn^{+3} and Mn^{+4} ions, and also has a significant A_3 peak. The latter is not present in the data for 30% Ca. The Ba and Pb preedges are slightly different; the Ba preedge features are not as well resolved even for the higher-energy resolution data while the A_1 peak is largest for the Pb sample (compare Fig. 6 with Fig. 5).

The most striking feature in Figs. 5 and 6 is the variation in the intensity of the preedge peaks and the shift of A_2 as T increases through T_c for the CMR samples. In contrast, the change for $LaMnO_3$ is small up to 300 K.[48] For the 21%-Ca sample in Fig. 5 the A_1 peak decreases in amplitude while the A_2 and B peaks increase with increasing T; the A_2 peak is sharpest at 300 K and clearly shifts downward below T_c (0.4–0.5 eV, depending on the background function used). See the solid triangles in Fig. 7. The change in the A peaks for the 33%-Ba sample (using the high-resolution monochromator) appear to follow the same trend as observed for the Ca data (Fig. 6) but the A_2 peak is not as well resolved.

The largest temperature dependence is observed for the $CaMnO_3$ sample above 300 K [see Fig. 5(a)], with the largest increase occurring for the B peak. Also, the amplitude of the peak at the top of the edge, commonly called the ''white line,'' [see Fig 1(c) at 6554 eV, for example] decreases slightly at high T. These effects become much larger at only slightly higher temperatures and will be treated in a separate paper. For the CMR samples, we associate the temperature-dependent changes in the amplitude of the preedge features with changes in charge localization/hybridization.

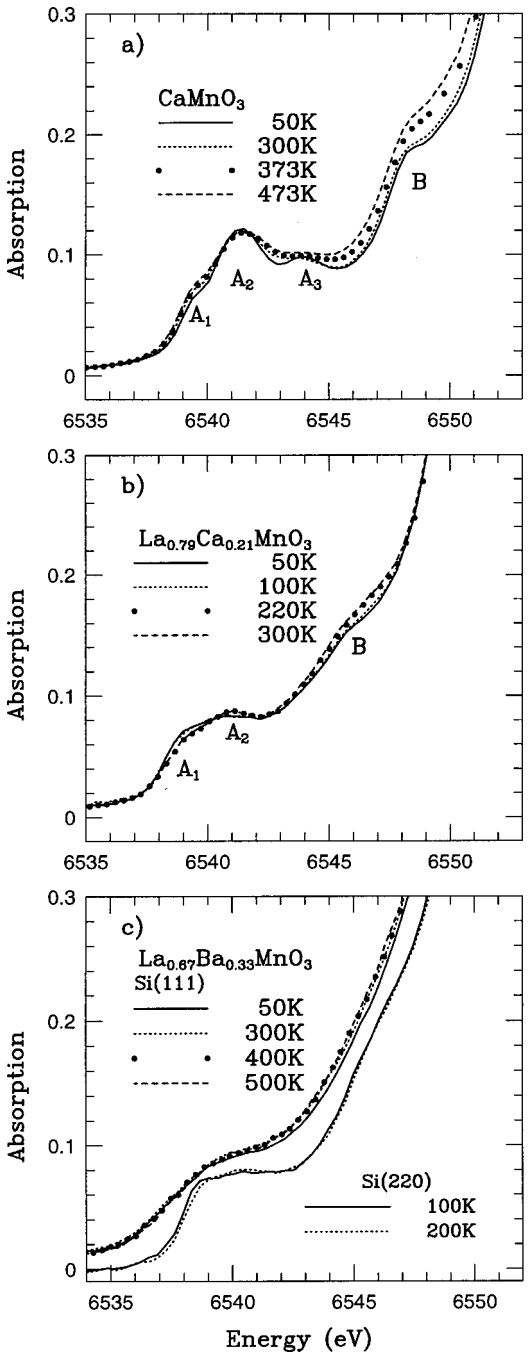

FIG. 5. The temperature dependence of the preedge region for $CaMnO_3$, 21% Ca, and 33% Ba; note different temperature ranges. The $CaMnO_3$ sample shows little change of the preedge region below 300 K while the A_1 and A_2 peaks are temperature dependent for the CMR samples. The Ba preedge data, collected using Si(220), are much sharper than data collected using Si(111) crystals, and show a splitting of the A peak. Note that the data collected using Si(220) in (c) have been shifted down by 0.15 eV for clarity.

C. Difference Spectra

More detailed information can be obtained by examining the change in the shape of the XANES region as a function of temperature. The files are first shifted to correct for any small changes in the energy of the monochromator and all

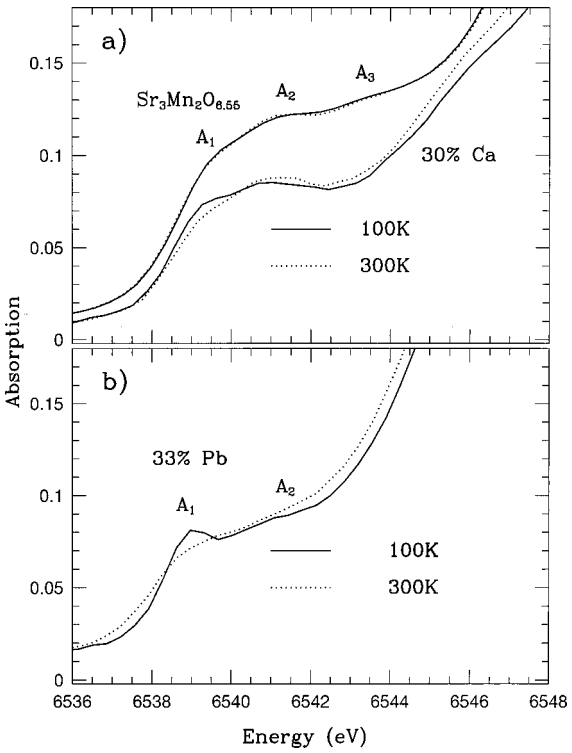

FIG. 6. The temperature dependence of the preedge region for $La_{0.7}Ca_{0.3}MnO_3$, $Sr_3Mn_2O_{6.55}$, and the 33%-Pb samples up to roughly 300 K. The leading edge of the A_1 peak is broader for $Sr_3Mn_2O_{6.55}$ than for the 30%-Ca sample in (a). In (b) the Pb samples have the largest A_1 peak at low *T*. Note that the scale is expanded compared to the previous figures and the B peak is not shown.

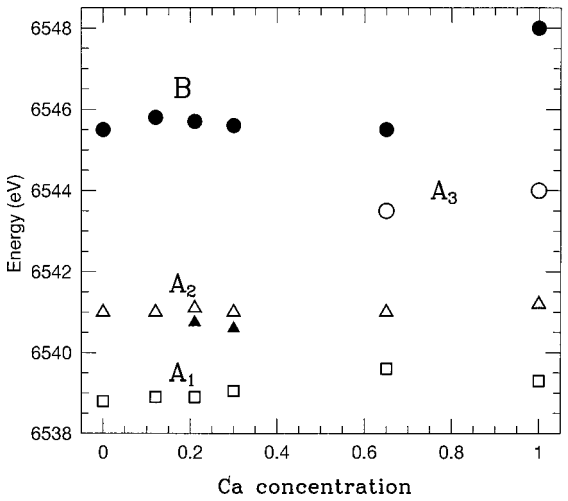

FIG. 7. The positions of the preedge features as a function of Ca concentration; open symbols; and solid circles, 300 K. The error in peak position is ± 0.1 eV. For the CMR samples, the A_2 peak is shifted to a lower energy for $T<T_c$. The filled triangles are for 50 K.

spectra are carefully normalized as discussed earlier. The difference spectra are obtained by subtracting the data at 300 K from all the data files (at different temperatures) for a given sample. This approach was used originally to investigate the preedge region for the 21% sample,[48] but considerable structure was found at energies corresponding to the main edge for both the CMR and CO ($x=0.65$) samples. Several examples of these difference spectra are shown in Fig. 8 for $LaMnO_3$ and $CaMnO_3$, and the 21, 30, and 65% Ca-substituted samples.

In the preedge region, the temperature variation of the A_1 and A_2 peaks for the 21 and 30% Ca (CMR) samples is very clearly visible in Figs. 8(c) and 8(d); it begins at T_c, with most of the change occurring over a 60-K range just below T_c. The temperature-dependent changes of the preedge are comparable in both samples, with the magnitude of the change of the A_2 peak being roughly 50–70 % that of the A_1 peak. For the 65%-Ca sample, changes of the A_1 with *T* are also observed in the difference spectra, but the amplitudes are considerably smaller, and interestingly, the phase is inverted—the A_1 difference peak decreases instead of increasing. For the $LaMnO_3$ sample [Fig. 8(a)] there is essentially no structure in the difference spectra over the preedge energy range, but surprisingly there are small peaks in this range for $CaMnO_3$ [see the lower part of Fig. 8(a)], with the largest peak in the difference spectra occurring *between* A_2 and A_3. This suggests that there are in reality more than three preedge peaks.

There is also well-defined structure in the difference spectra over the energy range of the main edge, although it is only a few percent of the edge in amplitude. For $LaMnO_3$ there is a broad feature over most of the edge region that increases as *T* is lowered. $CaMnO_3$ has a similar feature but it is larger and narrower [Fig. 8(a)]. Both appear to correspond to the temperature-dependent peak near the top of the edge (the ''white line'' mentioned earlier), which is sharpest at low *T*. For the CMR samples, there is additional structure on top of this broad peak—a dip at 6551 and a peak at 6553 eV (2 eV apart). Another dip/peak occurs just above the edge at 6555–6556.5 eV. The CO sample also shows structure over this energy range but again the phase is inverted relative to the CMR samples (i.e., a peak/dip at 6552 and 6554 eV). This phase inversion thus extends over the entire near-edge region.

IV. DISCUSSION

A. Main edge

For Mn atoms the main *K*-absorption edge represents transitions mainly from the atomic 1*s* state to the empty Mn *p* bands. The XANES results show that this edge is very sharp for the Ca-substituted samples, the O-excess samples, and the La-deficient sample. The width of the edge (roughly 5–6 eV) is narrower than the edge for most other Mn compounds and the average shift in edge position is ~ 3 eV for a valence change of $+1$. No obvious indication of a step or double edge structure is present that would indicate two distinct valence states. If completely localized Mn^{+3} and Mn^{+4} ions were present on time scales of 10^{-14} sec, the edge should have a smaller average slope and generally be broader, as would be expected for a mixture of fine powders

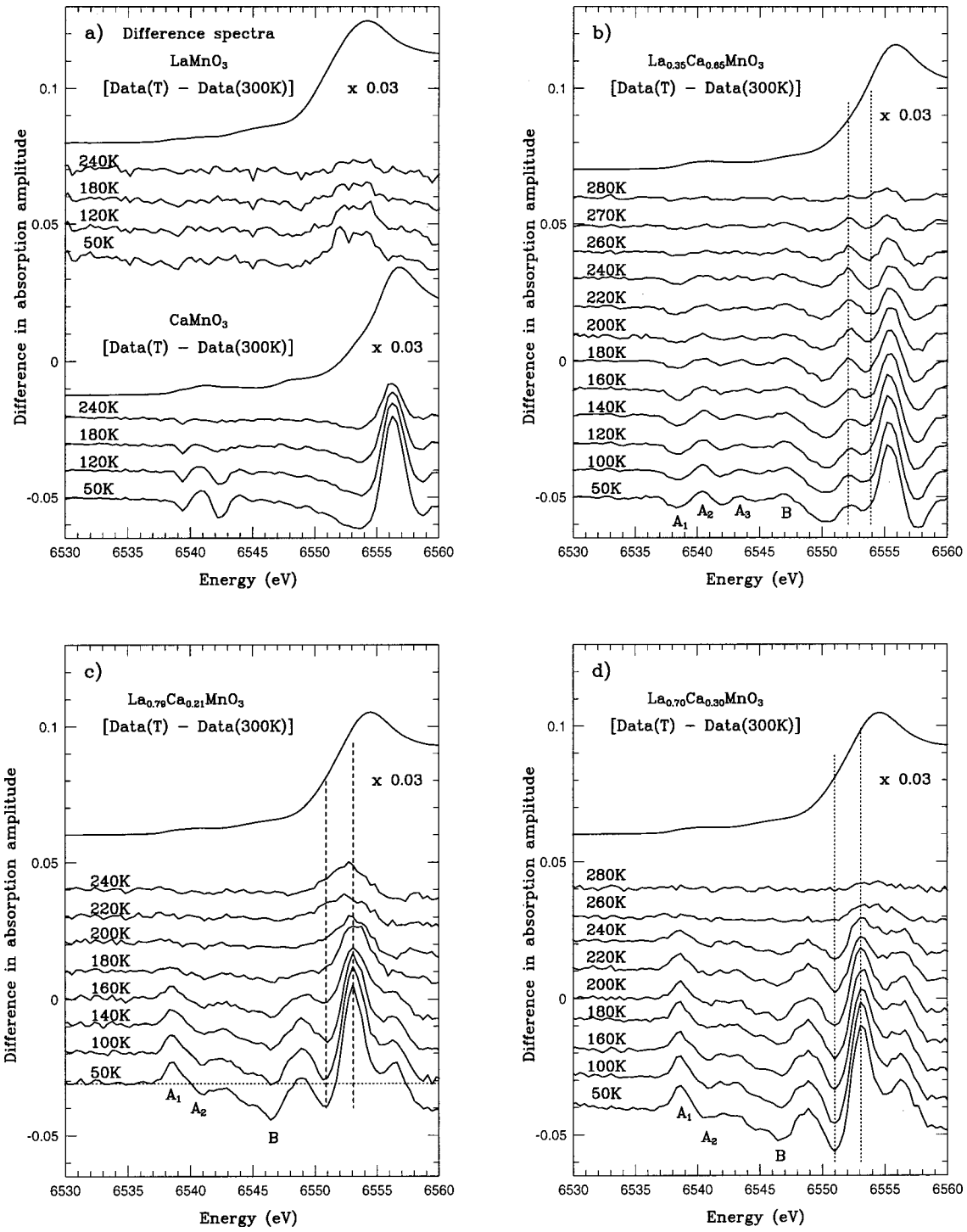

FIG. 8. The difference spectra as a function of temperature for 21, 30, and 65% Ca, and the end compounds. The main edge is included above each set of traces (multiplied by 0.03 to fit on the graph) to show where the structure is located relative to the edge. Note the inversion of the structure for the CO sample (b) ($T_{CO}=270$ K), compared to the CMR samples (c) (21% Ca, $T_c\sim 190$ K) and (d) (30% Ca, $T_c\sim 260$ K).

of $LaMnO_3$ and $CaMnO_3$. To model this explicitly, we compare in Fig. 9 the experimental edge for the 65%-Ca (CO) sample and a weighted sum of the +3 and +4 end compounds; clearly the experimental edge is much sharper as noted previously for CMR samples.[15,16]

In contrast to the Ca-doped samples, the edge for $Sr_3Mn_2O_{6.55}$ is much broader [Fig. 1(a)], with a width of ~ 10 eV. There is also a change of slope of the main edge for this sample that is consistent with two valence states, but the shape is more complicated. Note that a combination of two edges each ~ 5-eV wide, separated by ~ 3 eV (the separation for a valence change of 1) would yield an edge of width $\sim 8-9$ eV. Thus the width and structure of the $Sr_3Mn_2O_{6.55}$ edge are both consistent with the expectation

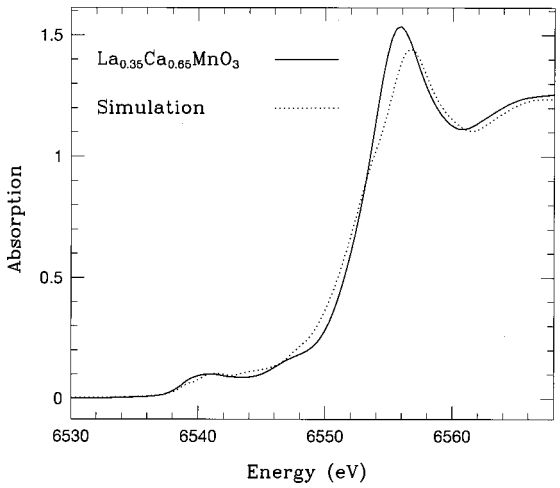

FIG. 9. A comparison of the data for the 65%-Ca sample and a simulation obtained from a 35–65 % weighted sum of the $LaMnO_3$ and $CaMnO_3$ end compounds. The experimental edge is significantly sharper.

that two valence states are present in this sample, Mn^{+3} and Mn^{+4}. Similarly our data for Mn_3O_4, which has a mixture of +2 and +3 valence states, has a very broad edge of 13–14 eV (not shown).

The edges for the Ba and Pb samples are also broader; they have a break in slope and more amplitude in the lower part of the edge that might suggest two valence states. This is quite different from the Ca-substituted samples for which the shape of the main edge for the CMR samples does not change much from that of $LaMnO_3$. In addition, the net shifts of the edges for the 33%-Ba and Pb samples are smaller than expected; the additional structure near 6546–6552 eV shifts the lower part of the edge down in energy while the top of the edge is close to the position of the 30%-Ca samples. The net result is a very small overall average edge shift compared to $LaMnO_3$. Thus the presence of Ba or Pb is directly affecting the Mn absorption edge although the average valence should be the same.

We have also shown by fitting over most of the edge, that there is no significant change in the average edge position for any of the substituted manganite samples near T_c. This agrees with our earlier result[15] in which we averaged data points above and below T_c. The new analysis also indicates that there is consistently a slight decrease in edge position at the highest temperatures that is largest for $CaMnO_3$ and $Sr_3Mn_2O_{6.55}$. The reason for this downward shift is not yet clear but may be related to the temperature dependence of the B peak (since an increase in the B-peak intensity effectively shifts the lower section of the edge to lower energy).

However, the lack of any temperature dependence below T_c disagrees slightly with the earlier work of Subías *et al.*,[16] who report a small 0.1-eV decrease in edge position up to T_c for $La_{0.6}Y_{0.07}Ca_{0.33}MnO_3$ and then a 0.09-eV increase up to 210 K. The small change in the shape of the main edge in Fig. 8 provides a partial explanation for this discrepancy. Subías *et al.* assumed no change in edge shape and calculated difference spectra for each temperature. Under this assumption, the amplitude of the peak in the difference spectra would be proportional to the energy shift of the edge. The additional structure observed in the difference spectra indicates there is a shape change rather than an overall edge shift.

The structure in the difference spectra (Fig. 8) is clearly correlated with T_c. For the CMR samples, the dip-peak structure, superimposed on the peak observed for the end compounds, begins to be observable near T_c and grows rapidly in the 60–100 K range just below T_c. This structure means that compared to the edge at low temperatures (undistorted Mn-O bonds) the edge above T_c (distorted Mn-O bonds) has the upper part of the edge shifted upward in energy while the lower part is shifted downwards. The separation between the dip-peak structure is about 2 eV (see vertical dotted lines).

This brings us to the questions raised in the Introduction—is there a mixture of +3 and +4 sites as usually assumed? If so, why is the edge structure so small? One possibility is that the system is more covalent[15,16,19,20] and that there are some partial holes in the O $2p$ band that are hybridized with the Mn $3d$ states. This is supported by several calculations and by the observation of holes in the O $2p$ band in absorption studies.[28] Such holes may play an important role in the unusual transport of these materials. In calculations, Anisimov *et al.*[22] and Mizokawa and Fujimori[23] obtain two types of Mn e_g configurations with almost identical local charge densities. From this perspective, the charge added via Ca doping is spread over several atoms and the variation of the local charge on different Mn atoms may be small. Thus covalency can partially explain the lack of structure in the edge, while at the same time the average edge position increases roughly linearly with dopant concentration. The recent calculations of Elfimov *et al.*[30] are also relevant in this regard. To fit the observed splittings of the A_1 peaks (2.2 eV for $LaMnO_3$ and 1.8 eV for $CaMnO_3$), U and J_H had to be lowered from the values in the first calculation[30] to 4 and 0.7 eV, respectively,[48] which implies higher covalency.

However, many experiments also show that the CMR samples are distorted above T_c but ordered at low T. Since long and short bond lengths generally correspond to different edge positions,[29] why does that not produce a significant change in the shape of the edge with temperature—i.e., why is the tiny structure observed so small? In the calculations mentioned above there are also distortions of the Mn-O bond distances. For example, in the calculation of Anisimov *et al.*,[22] one configuration is symmetric in the ab plane with four small equal lobes directed towards O while the other has two large (and two small) lobes, again directed towards O atoms in the ab plane, which leads to two distinct Mn-O distances. The more symmetric case has been associated with a formal Mn^{+4} site and the other state with Mn^{+3}.

For the manganites, both Elfimov *et al.*[30] using LSDA and Benfatto *et al.*[31] using multiple-scattering calculations have shown explicitly that the Mn *K*-edge is bond-length dependent. It occurs at a lower energy when the Mn-O bond lengthens (p_x orbitals in Ref. 30 and p_y orbitals in Ref. 31) and is at a higher energy for shorter bond lengths, with a

separation of about 2 eV, which is about 70% that expected for a full valence shift of 1 unit. The experimental dip-peak splitting is also about 2 eV; in light of the fact that both calculations give the same value, we propose that the structure we observe is direct evidence for this splitting in the manganites. However, the unanswered question is why the amplitude is so small. The experimental dip-peak structure has an amplitude of only $\sim 2\%$, whereas a similar measurement for the difference between the simulation and the data in Fig. 9 would have an amplitude over 30% (and the difference using the simulation in Ref. 16 for 33% Ca would be over 10%).

Since the distortions are well verified, can the small amplitude of the structure observed in the difference spectra be explained in some other way? Here we first need to digress briefly to describe the situation more carefully. The $1s$ absorption edge is a transition into states of p symmetry that become a continuum well above the edge. Many investigators, including those of Refs. 30 and 31, attribute the *K*-edge absorption to Mn $1s$-$4p$ transitions (broadened by the core-hole lifetime), but in principle many other p states could contribute and are included automatically in the multiple-scattering approach. In band-structure calculations the Mn partial p density of states (DOS) can be projected out. The $4p$ partial DOS describes the absorption edges for transition metals quite well, while the $5p$ partial DOS has little contribution near the absorption edge.[49] As an example, the shape of the projected $4p$ DOS in the calculation of Elfimov *et al.*[30] for the manganites is very similar to that observed experimentally.[48] It is therefore a useful simplification, and in light of the success of a number of band theory calculations, probably not a bad approximation, to consider only the Mn $4p$ partial DOS in a tight-binding model for the rest of this discussion.

In the paper by Elfimov *et al.*[30] the Mn $4p$ DOS is very wide, roughly 20 eV, which signifies that the states are strongly interacting. This means the Mn $4p$ orbitals overlap significantly and hence the radial extent of the Mn $4p$ orbitals must be large. The overlap with the O atoms is also large and leads to the sensitivity of the edge position to the Mn-O bond lengths as calculated.[30,31] Furthermore the large band width also implies that the core-hole-conduction electron Coulomb interaction is not very important, i.e., that a small local potential does not affect the broad $4p$ band. The fact that Elfimov *et al.* and Benfatto *et al.* obtain identical results for the effect of the Mn-O bond lengths on the respective p_x, p_y edge positions in $LaMnO_3$ (a shift of 2eV) supports this notion, as the core hole is included in the multiple scattering but not the LDA calculations.

In $LaMnO_3$, there are rows of long Mn-O bonds along the c axis and rows of shorter bonds along the a and b axes. Consequently, the Mn $4p$ overlap will be larger along the a and b axes than on the c axis, which leads to the 2-eV shift of the edge of the $4p$ DOS along the different axes. However for the mixed compounds $La_{1-x}Ca_xMnO_3$, the situation is quite different as there can be various combinations of long and short bonds along a given axis. Statistically there will only be a small number of situations where there are all long (i.e., three neighboring Mn atoms with J-T distortions along the same axis) or all short bonds in a row, but many cases with a mixture of long and short bonds. This will greatly reduce the structure in the absorption edge—the 2-eV splitting remains but the fraction of Mn atoms with the high- or low-energy edges is small. The large overlap also implies that valence effects are averaged, i.e., that the difference in the projection of $4p$ states onto Mn atoms that are considered to be $+3$ or $+4$ is small. We thus propose that the small amplitude in the structure in the Mn *K* edge is a combination of increased covalency and the net averaging over more than one Mn site as described above from band-structure effects. Because the usual approach in XANES studies is to assume a very localized excitation, more work will be needed to determine to what extent band structure contributes.

For the CO sample there is also structure in the edge but the phase is inverted. If the above explanation for the *dip-peak* structure in the difference spectra for CMR samples is correct then it suggests that the *peak-dip* feature for the CO sample is also produced by local distortions—but in this case by a local distortion that starts at the charge ordering temperature $T_{CO}=270$ K, and *increases* as T is lowered. Such a model then provides a simple interpretation for the unusual lack of temperature dependence (reported[15] but not explained) for σ^2 for this sample. The surprise is that at least the thermal phonon broadening should have caused some increase in σ^2 with T. However, if there is a distortion associated with the CO state, then there must be an associated broadening contribution σ_{CO} for the Mn-O pair distribution function σ^2_{CO} that is zero above T_{CO} and increases as T is lowered below T_{CO}. Then the total variance for the Mn-O bond σ^2_{Mn-O} will be given by

$$\sigma^2_{Mn-O}(T)=\sigma^2_{phonon}(T)+\sigma^2_{CO}(T)+\sigma^2_{static}, \qquad (1)$$

where $\sigma^2_{phonon}(T)$ is the phonon contribution and σ^2_{static} is a static (temperature-independent) contribution from disorder. $\sigma^2_{phonon}(T)$ should be comparable to that for $CaMnO_3$, since we see the same phonon component for both pure $CaMnO_3$ and $La_{0.79}Ca_{0.21}MnO_3$ above T_c. To make σ^2_{total} nearly independent of T means $\sigma^2_{CO}(T)$ and $\sigma^2_{phonon}(T)$ almost cancel for temperatures below 300 K.

We can extract the CO contribution following the method in Ref. 15 for calculating $\Delta\sigma^2$. We fit the two highest-T data points (from Ref. 15) to $\sigma^2_{phonon}(T)+\sigma^2_{static}$ and then subtract these contributions from the data. In Fig. 10 we plot the result of this analysis for the 65%-Ca sample. From this figure, the maximum value for $\sigma^2_{CO}(T)$ is roughly 10% of that associated with polaron formation for the CMR samples. Such an increased distortion for charge ordered material makes sense—as the sample becomes charge or orbital ordered, there is more room for the longer Mn-O bonds to lengthen, which increases some of the Mn-Mn distances and shifts the corresponding $4p$ DOS down in energy, while for a random arrangement of orbitals, the series of long and short Mn-O bonds are more constrained.

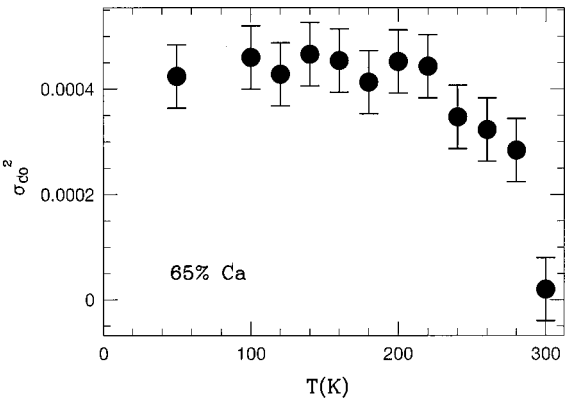

FIG. 10. A plot of $\sigma^2_{CO}(T)$ for the Mn-O bond as a function of T (65%-Ca sample). $\sigma^2_{CO}(T)$ is extracted from the $\sigma^2_{Mn-O}(T)$ data presented in Ref. 15. $T_{CO}\sim 270$ K.

B. Pre-edge region

1. Background

The preedge results provide additional information about the nature of the electronic states. For many of the transition elements, one to three preedge peaks A_i, occur well below the main edge (~ 15 eV below) and are assigned to transitions to empty states with *d*-like character, i.e., these are $1s$ to $3d^{(n+1)}$ transitions[50,51] where n is the initial number of d electrons and $n+1$ includes the excited electron in the final state. As outlined in the Introduction, these peaks are predominantly $1s$-$3d$ transitions made weakly allowed via an admixture of $3d$ and $4p$ states.[33,32,35,37,48] In the preedge region there may also be some hybridization with the O $2p$ states. If the metal site is centrosymmetric, there is no mixing of $3d$ and $4p$ states on the excited atom and $1s$-$3d$ dipole transitions are strictly forbidden;[33] however local distortions can make such $1s$-$3d$ transitions very weakly dipole allowed. Three aspects need to be recognized in considering the Mn preedge in the present study.

Quadrupole interactions. Based on recent studies on oriented single crystals[32,34–37] we estimate that quadrupole-allowed peaks will be at most 1% in powder samples, which is considerably smaller than the A_i peaks observed for the substituted manganites but perhaps not negligible. A small quadrupole component, as seen for example in FeO,[37] may well be present.

Dipole allowed via 3d-4p mixing on the absorbing atom. If the Mn site lacks inversion symmetry, then in principle there will be mixing of the Mn $3d$ and $4p$ states on the central atom. Consider a system that is nearly cubic but has a small distortion that removes the inversion symmetry, i.e., the metal atom is slightly displaced such that the bonds on opposite sides of the metal atom are slightly different. Then the mixing parameter is $\sim \delta_l/r_o$ and the matrix element will be proportional to $(\delta_l/r_o)^2$, where δ_l is the difference in opposite bond lengths and r_o is the average bond length. An example is the V site in V_2O_5; here the VO_6 octahedron is strongly distorted[35,36] and along the *c* axis, the two V-O bond lengths are 1.577 and 2.791 Å , respectively. Experimentally there is a large preedge peak for the V *K* edge that can be modeled assuming $3d$-$4p$ mixing on the absorbing atom plus the effect of a corehole.

Dipole allowed via 4p mixing with neighboring metal atom 3d states. In several cases, a significant preedge peak is observed in a cubic crystal that can't be explained by the above $3d$-$4p$ mixing on the excited atom. Multiscattering calculations for such systems often show that large clusters are needed before the preedge features are produced—scattering paths are needed that include many further neighbors, particularly the second-neighbor metal atoms. An equivalent result emerges from band theory calculations where the hybridization of orbitals on different atoms is important. Here the dipole transition can be made allowed via mixing of the $4p$ state on the central atom with the $3d$ states on neighboring atoms. Projections of the density of states with p character (p DOS) for such systems show small features at the energies of the $3d$ states; such features are not observed in the p DOS when the preedge feature is a quadrupole transition. In the limit of multiscattering calculations with very large clusters, the two approaches (band theory and multiscattering) should be equivalent.

To have a mixing of $3d$ with the $4p$ states (to make a state of p character), one needs a combination of $3d$ states that has odd parity as pointed out by Elfimov *et al.*[30] It is easy to obtain such a state if a linear combination of $3d$ states on two neighboring Mn atoms is used and the radial extent of the Mn $4p$ states is large enough to overlap them. Specifically, consider three Mn atoms in a line—a central excited atom (0) and left (L) and right (R) atoms—with $\Psi_{4p}(0)$ being the $4p$ state on the central atom, and $\Psi_{3d;x^2-y^2}(R_R)$ and $\Psi_{3d;x^2-y^2}(R_L)$ being the $3d_{x^2-y^2}$ states centered on the right and left atoms. Then a state with odd symmetry about the central atom is given by

$$\Psi_{total}=\alpha\Psi_{4p}(0)+\frac{\beta}{\sqrt{2}}[\Psi_{3d;x^2-y^2}(R_L)-\Psi_{3d;x^2-y^2}(R_R)], \tag{2}$$

where α is essentially 1.0 and we ignore the intervening O atom via which the hybridization occurs. The small parameter β is a measure of the hybridization and is strongly dependent on the overlap of the $4p$ and $3d$ wave functions on different Mn atoms, and hence on the distance between them.

2. Application to the substituted manganites

The preedge for the substituted manganites follows the general trends observed for other Mn systems quite well. Three A peaks are observed for $CaMnO_3$; A_2 is larger than the A_1 peak, and the A_2-A_1 splitting is smaller (high valence $+4$) than for other samples. The $LaMnO_3$ case is similar; the A_2-A_1 splitting is largest (lower valence $+3$) and the overall A-peak amplitude is smallest. However, the A_2 peak is larger than expected from the literature for Mn^{+3} states in other compounds,[33] possibly because of increased local distortions in this compound.

However, there are difficulties with some of the earlier interpretations[38,33] in which the dipole-allowed transitions are assumed to originate from a 3d-4p mixing on the excited

atom. First the A_i peaks appear for both distorted and undistorted systems. Second, the amplitude (particularly for the relatively undistorted system $CaMnO_3$) is too large to be a $1s$-$3d$ transition made, allowed by a slight breaking of inversion symmetry about the excited Mn atom. Recently, based on the calculations of Elfimov *et al.*,[30] we have interpreted A_1 and A_2 as dipole allowed via a mixing of Mn $4p$ states with Mn $3d$ states on neighboring metal atoms.[48] The projected p DOS in the calculations of Elfimov *et al.*[30] show two features in the preedge region that indicate that dipole-allowed transitions should be present. In addition, the broad Mn $4p$ band obtained in that work (and implied in the calculation of Benfatto *et al.*[31]) indicates that the radial extent of the $4p$ states is indeed large—a necessary requirement for mixing with the $3d$ states on the neighboring metal atoms. Similar interpretations have been given recently for other transition-metal systems that are cubic or very nearly so; Fe in FeO (Ref. 37) and Ti in rutile.[32,34] A mixing with the $3d$ states on neighboring Ti atoms was also reported in the layered disulfide TiS_2.[52]

The calculations of Elfimov *et al.* also show that there is a splitting of the unfilled $3d$ bands. The lowest is the majority e_g band (which may be partially filled via doping); the next two are the minority e_g and t_{2g} bands that partially overlap. The coupling with the t_{2g} is expected to be smaller since these orbitals are of the form d_{xy}, which has reduced overlap with the Mn $4p$ in a π bonding configuration. The splitting of these e_g bands depends both on J_H and on the degree of covalency/hybridization.

Finally the temperature dependence of the A_i peak amplitudes is still not explained. The observation that the changes for the CO and CMR samples are inverted implies that these changes are related to the changes in the local distortions, but a detailed model is needed.

3. Other Models

Another general feature that emerges from our data is that although the main changes occur just below T_c, there is also a gradual change to the fully ordered state as the sample is cooled well below T_c, and the local structure continues to change down to 50 K and below. Consequently there may be clusters formed at T_c that grow as T is lowered. We have interpreted our local distortion results earlier in terms of a two-component model.[14] In this model, one of the components (fluids) would correspond to delocalized states—they could be either delocalized holes or delocalized electrons. We also point out that the decreasing distortions observed in extended XAFS as T is decreased below T_c and the corresponding increase in resistivity suggest a changing average mobility of the charge carriers. Within the model we have suggested, the fraction of delocalized carriers would increase as T is lowered.[15] Note that Jaime *et al.*[53] have successfully modeled their resistivity and thermoelectric measurements using a two-component system of localized and itinerant carriers. However, one of the components in our model might also correspond to the Mn atoms in a cluster, the positions of which are dominated by small variations in dopant concentration or O vacancies, possibly leading to a regime with phase separation. Such inhomogeneities likely play an important role in these materials. The recent calculations using the Kondo model[54–56] also stress phase separation but it is not clear how to compare with their results.

V. CONCLUSIONS

We have addressed several issues related to the Mn valence in the substituted $LaMnO_3$ materials, including the nature of the transition and some differences between band theory and multiple-scattering approaches. Although discussions of these systems often assume isolated Mn^{+3} and Mn^{+4} states, we observe no change (<0.02 eV) in the average edge position through the ferromagnetic transition for the CMR systems (Ca, Ba, or Pb doped), and in all cases the total edge shift from 0–300 K is <0.04 eV. Although there is no obvious step or kink in the edge, expected for two well-defined valence states, there is a very small shape change that can be observed by taking the difference of data files at different temperatures. A dip/peak structure develops as T drops below T_c for the CMR samples; the dip/peak separation is ~ 2 eV and agrees with the 2-eV splitting calculated[30,31] for the p_x and p_y partial DOS when the manganite structure changes from an undistorted to a distorted ($LaMnO_3$) lattice. For CMR samples, such changes in the local distortions below T_c were deduced earlier from EXAFS data.[13–16] At low T the CMR samples are very well ordered, but as T increases there is a rapid increase in the local distortions up to $T=T_c$; above T_c the change in disorder changes slowly. The rapid change just below T_c has been associated with the formation of polarons. These distortions, now observed in both the XANES and EXAFS data, indicate some change in the local charge distribution. However the small size of the effect in the XANES spectra needs to be understood. In part it can be attributed to covalency with the charge shared between the Mn and O atoms. However the different bond lengths should also yield structure in the edge but experimentally it is very small. We propose that because of the large radial extent of Mn $4p$ orbitals (indicated by the broad Mn $4p$ bandwidth), the $1s$-p edge transition may be averaged as a result of band theory effects. Future XANES studies will be necessary to evaluate this possibility more fully.

For the CO sample we observe a similar behavior, but in this case the structure in the difference spectra are inverted relative to that for the CMR sample. This indicates that the local distortions increase in the CO state below T_{CO}.

The preedge structure provides additional information about the $3d$ bands in these materials. Two or three peaks are observed, labeled A_1–A_3. A_2 at 300 K is essentially independent of concentration while A_1 increases slowly with x; A_3 is only observed for high-Ca concentrations. Following the work of Elfimov *et al.*[30] we attribute these peaks to a hybridization of Mn $4p$ on the excited atom with an ungerade combination of $3d$ states on neighboring Mn atoms, i.e., they are not the result of splittings of atomic multiplets on the excited atom as is often assumed. Similar explanations for the preedge region have recently been proposed for several other transition-metal K edges. Conse-

quently the splittings observed are essentially unaffected by the presence of the core hole and should be a good measure of the splittings of the e_g bands that are influenced by the hybridization of the Mn $3d$ and O $2p$ states. This interpretation of the preedge does not depend on small distortions of the crystal and therefore also provides a simple explanation for the large preedge features observed in the more ordered $CaMnO_3$ material.

In the calculations of Elfimov *et al.*,[30] the two lowest empty bands are the majority- and minority-spin e_g bands; the minority-spin t_{2g} band overlaps the latter but is expected to be more weakly coupled. U and J must be reduced slightly to fit the experimental splitting (2 eV) of the A_1 and A_2 peaks; $U=4$ and $J_H=0.7$ eV. This indicates an increase in the covalency. The additional small decrease in the A_1-A_2 splitting below T_c may suggest a further change in covalency or hybridization.

Thus the picture that emerges is that there is considerable hybridization of the energy states (Mn $4p$ and $3d$, and O $2p$), with some hole density in the O bands and possibly only small differences in the charge localized on Mn atoms that have different types of e_g orbitals. The possibility of distinct types of orbitals can lead to orbital ordering,[22] with displacements of the O atoms forming J-T-like Mn-O bond distortions when the hopping charge is localized for times of order the optical phonon periods. As a result, the possibility that part of the transport takes place via hole density in the O bands needs to be considered. Note that slowly hopping holes on the O sites would lead to distorted Mn-O bonds while rapid hopping (faster than phonons) would leave the O atom at an average undistorted position.

ACKNOWLEDGMENTS

The authors wish to thank G. Brown, C. Brouder, D. Dessau, T. Geballe, J. Rehr, G. Sawatzky, and T. Tyson for useful discussions and comments. F.B. thanks K. Terakura for sending some unpublished results. The experiments were performed at the Stanford Synchrotron Radiation Laboratory, which is operated by the U.S. Department of Energy, Division of Chemical Sciences, and by the NIH, Biomedical Resource Technology Program, Division of Research Resources. Some experiments were carried out on UC/National Laboratories PRT beam time. The work was supported in part by NSF Grant No. DMR-97-05117.

[1] J. Volger, Physica (Amsterdam) **20**, 49 (1954).
[2] E. O. Wollan and W. C. Koehler, Phys. Rev. **100**, 545 (1955).
[3] P. Schiffer, A. P. Ramirez, W. Bao, and S-W. Cheong, Phys. Rev. Lett. **75**, 3336 (1995).
[4] G. H. Jonker and J. H. van Santen, Physica (Amsterdam) **16**, 337 (1950).
[5] A. P. Ramirez, P. Schiffer, S-W. Cheong, C. H. Chen, W. Bao, T. T. M. Palstra, P. L. Gammel, D. J. Bishop, and B. Zegarski, Phys. Rev. Lett. **76**, 3188 (1996).
[6] C. H. Chen, S-W. Cheong, and H. Y. Hwang, J. Appl. Phys. **81**, 4326 (1997).
[7] C. Zener, Phys. Rev. **82**, 403 (1951).
[8] P. W. Anderson and H. Hasegawa, Phys. Rev. **100**, 675 (1955).
[9] P. G. de Gennes, Phys. Rev. **118**, 141 (1960).
[10] A. J. Millis, P. B. Littlewood, and B. I. Shraiman, Phys. Rev. Lett. **74**, 5144 (1995).
[11] A. J. Millis, B. I. Shraiman, and R. Mueller, Phys. Rev. Lett. **77**, 175 (1996).
[12] H. Röder, J. Zang, and A. R. Bishop, Phys. Rev. Lett. **76**, 1356 (1996).
[13] C. H. Booth, F. Bridges, J. B. Boyce, T. Claeson, B. M. Lairson, R. Liang, and D. A. Bonn, Phys. Rev. B **54**, 9542 (1996).
[14] C. H. Booth, F. Bridges, G. H. Kwei, J. M. Lawrence, A. L. Cornelius, and J. J. Neumeier, Phys. Rev. Lett. **80**, 853 (1998).
[15] C. H. Booth, F. Bridges, G. H. Kwei, J. M. Lawrence, A. L. Cornelius, and J. J. Neumeier, Phys. Rev. B **57**, 10 440 (1998).
[16] G. Subías, J. García, M. G. Proietti, and J. Blasco, Phys. Rev. B **56**, 8183 (1997).
[17] S. J. L. Billinge, R. G. DiFrancesco, G. H. Kwei, J. J. Neumeier, and J. D. Thompson, Phys. Rev. Lett. **77**, 715 (1996).
[18] N. Nücker, J. Fink, J. C. Fuggle, P. J. Durham, and P. J. Temmerman, Phys. Rev. B **37**, 5158 (1988).
[19] M. Croft, D. Sills, M. Greenblatt, C. Lee, S.-W. Cheong, K. V. Ramanujachary, and D. Tran, Phys. Rev. B **55**, 8726 (1997).
[20] T. A. Tyson, Q. Qian, C.-C. Kao, J.-P. Rueff, F. M. F. deGroot, M. Croft, S.-W. Cheong, M. Greenblatt, and M. A. Subramanian, Phys. Rev. B **60**, 4665 (2000).
[21] W. E. Pickett and D. J. Singh, Phys. Rev. B **53**, 1146 (1996).
[22] V. I. Anisimov, I. S. Elfimov, M. A. Korotin, and K. Terakura, Phys. Rev. B **55**, 15 494 (1997).
[23] T. Mizokawa and A. Fujimori, Phys. Rev. B **56**, R493 (1997).
[24] P. Dai, J. D. Zhang, H. A. Mook, S.-H. Liou, P. A. Dowben, and E. W. Plummer, Phys. Rev. B **54**, 3694 (1996).
[25] G. Zhao, K. Conder, H. Keller, and K. A. Müller, Nature (London) **381**, 676 (1996).
[26] J.-S. Zhou, J. B. Goodenough, A. Asamitsu, and Y. Tokura, Phys. Rev. Lett. **79**, 3234 (1997).
[27] G. H. Kwei, D. N. Argyriou, S. J. L. Billinge, A. C. Lawson, J. J. Neumeier, A. P. Ramirez, M. A. Subramanian, and J. D. Thompson, in *Magnetic Ultrathin Films, Multilayers, and Surfaces*, edited by J. Tobiu, D. Chambliss, D. Kubinski, and D. Bormak, MRS Symposia Proceedings No. 475 (MRS, Pittsburgh, 1997), p. 533.
[28] H. L. Ju, H.-C. Sohn, and K. M. Krishnan, Phys. Rev. Lett. **79**, 3230 (1997).
[29] A. Bianconi, in *X-ray Absorption: Principles, Applications, Techniques of EXAFS, SEXAFS and XANES*, edited by D. C. Koningsberger and R. Prins (Wiley, New York, 1988), p. 594.
[30] I. S. Elfimov, V. I. Anisimov, and G. A. Sawatzky, Phys. Rev. Lett. **82**, 4264 (1999).
[31] M. Benfatto, Y. Joly, and C. R. Natoli, Phys. Rev. Lett. **83**, 636 (1999).
[32] Y. Joly, D. Cabaret, H. Renevier, and C. R. Natoli, Phys. Rev. Lett. **82**, 2398 (1999).

[33] A. Manceau, A. I. Gorshkov, and V. A. Drits, Am. Mineral. **77**, 1133 (1992).
[34] Y. Aïfa, B. Poumellec, V. Jeanne-Rose, R. Cortes, R. V. Vedrinskii, and V. L. Kraizman, J. Phys. IV **7**, C2 (1997).
[35] B. Poumellec, V. Kraizman, Y. Aifa, R. Cortès, A. Novakovich, and R. Vedrinskii, Phys. Rev. B **58**, 6133 (1998).
[36] O. Sipr, A. Simunek, S. Bocharov, T. Kirchner, and G. Dräger, Phys. Rev. B **60**, 14 115 (1999).
[37] D. Heumann, G. Dräger, and S. Bocharov, J. Phys. IV **7**, C2 (1997).
[38] M. Belli, A. Scafati, A. Bianconi, S. Mobilio, L. Pallandino, A. Reale, and E. Burattini, Solid State Commun. **35**, 355 (1980).
[39] S. Satpathy, Z. S. Popović, and F. R. Vukajlović, Phys. Rev. Lett. **76**, 960 (1996).
[40] G. J. Snyder, R. Hiskes, S. DiCarolis, M. R. Beasley, and T. H. Geballe, Phys. Rev. B **53**, 14 434 (1996).
[41] J. Mitchell, J. E. Millburn, M. Medarde, S. Short, and J. D. Jorgensen, J. Solid State Chem. **141**, 599 (1998).
[42] M. E. Leonowicz, K. R. Poeppelmeier, and J. Longo, J. Solid State Chem. **59**, 71 (1985).
[43] G. Subías, J. García, J. Blasco, and M. G. Proietti, Phys. Rev. B **57**, 748 (1998).
[44] I. Maurin, P. Barboux, Y. Laissailly, J. P. Boilot, and F. Villain (unpublished).
[45] R. S. Liu, L. Y. Jang, J. M. Chen, Y. C. Tsai, Y. D. Hwang, and R. G. Liu, J. Solid State Chem. **128**, 326 (1994).
[46] H. Yamaguchi, A. Yamada, and H. Uwe, Phys. Rev. B **58**, 8 (1998).
[47] T. Ressler, J. Wong, J. Roos, and I. Smith, Environ. Sci. Technol. **34**, 950 (2000).
[48] F. Bridges, C. H. Booth, G. H. Kwei, J. J. Neumeier, and G. A. Sawatzky, Phys. Rev. B **61**, R9237 (2000).
[49] G. Sawatzky (private communication).
[50] J. S. Griffith, in *The Theory of Transition Metal Ions* (Cambridge University Press, Cambridge, England, 1961).
[51] S. Sugano, Y. Tanabe, and H. Kamimura, in *Multiplets of Transition-Metal Ions* (Academic Press, New York, 1970).
[52] Z. Y. Wu, G. Ouvrard, P. Moreau, and C. R. Natoli, Phys. Rev. B **55**, 9508 (1997).
[53] M. Jaime, P. Lin, S. H. Chun, M. B. Salamon, P. Dorsey, and M. Rubinstein, Phys. Rev. B **60**, 1028 (1999).
[54] S. Yunoki, J. Hu, A. L. Malvezzi, A. Moreo, N. Furukawa, and E. Dagotto, Phys. Rev. Lett. **80**, 845 (1998).
[55] S. Yunoki and A. Moreo, Phys. Rev. B **58**, 6403 (1998).
[56] E. Dagotto, S. Yunoki, A. L. Malvezzi, A. Moreo, and H. Ju, Phys. Rev. B **58**, 6414 (1998).